Available online at www.sciencedirect.com
SCIENCE DIRECT
Polymer 46 (2005) 6543–6553
polymer
www.elsevier.com/locate/polymer

Correlating the rheological and mechanical response of polyurethane nanocomposites containing hyperbranched polymers

Christopher J.G. Plummer[a], Marlene Rodlert[a], Jean-Luc Bucaille[a], Henri J.M. Grünbauer[b], Jan-Anders E. Månson[a,*]

[a]*Laboratoire de Technologie des Composites et Polymères (LTC), École Polytechnique Fédérale de Lausanne (EPFL), Station 12, CH-1015 Lausanne, Switzerland*
[b]*Dow Benelux N.V., New Business Dev., NL-4530 AA, Terneuzen, Netherlands*

Available online 26 May 2005

Abstract

Cast polyurethane thermosets have been modified with randomly oriented exfoliated and intercalated montmorillonite clay using hyperbranched polymers (HBP) as reactive additives to promote dispersion of the clay platelets. The influence of the clay content on the stiffness of the nanocomposites is discussed in terms of simplified classical micromechanical models that allow correlations to be established between the properties of the final polyurethane and the limiting high strain rate shear viscosity of the HBP or HBP/polyethylene glycol nanocomposite precursors. Such models imply certain restrictions on the potential for mechanical reinforcement with unoriented platelets owing to crowding effects. Moreover, they appear unable to account simultaneously for the observed degrees of reinforcement in the glassy and the rubbery states, if currently accepted values for the stiffness of the MMT are assumed. Possible reasons for this are discussed.

Keywords: Nanocomposites; Polyurethane; Hyperbranched polymers

1. Introduction

Naturally occurring smectite clays such as Na^+ montmorillonite (MMT) typically consist of micron-sized stacks of negatively charged platelets bound by interlayer cations. If these layers can be fully dispersed, that is, 'exfoliated' in a polymer matrix, the physical and mechanical properties of the resulting nanocomposite may be significantly improved with respect to those of the unmodified matrix, even at relatively low MMT contents [1–6]. The combination of a large specific polymer–clay interfacial area, constraints on the matrix mobility close to the interface and changes in the matrix morphology have frequently been invoked to explain these improvements, particularly in the case of polyamide/MMT nanocomposites [2,7]. However, the observed mechanical reinforcement may at least to some extent be accounted for by the stiffness and high aspect ratios, α, of the individual MMT platelets [8–10]. High α ensure efficient stress transfer between the platelets and the matrix in the presence of strong interfacial interactions, which are usually a prerequisite for exfoliation [11–13].

Exfoliated and/or intercalated MMT nanocomposites have been reported for a wide variety of polymer matrices, including polyurethane (PUR) thermosets [14–18]. As with many such materials, work on PUR-based nanocomposites is often driven by the prospect of significantly improved mechanical properties at MMT contents of as little as a few weight percent, and this has provided the focus for the investigation described in what follows. Nevertheless, other potential benefits, such as improved flame retardance, may prove to be of equal if not greater practical interest in the long term, since it remains to be seen whether significant MMT reinforcement is compatible with conventional thermoset technology, particularly if the final product is in the glassy state. Two important issues in this context are the influence of the MMT on the viscosity of the resin and control of the platelet orientation, particularly in castings. This presupposes that adequate platelet dispersions can be obtained. In the present case various degrees of exfoliation have been achieved by incorporating –OH terminated hyperbranched polyesters (HBPs) into the polyol precursor along with the MMT. HBPs, for which a representative

* Corresponding author. Tel.: +41 21 693 4281; fax: +41 21 693 5880.
E-mail address: jan-anders.manson@epfl.ch (J.-A.E. Månson).

0032-3861/$ - see front matter © 2005 Elsevier Ltd. All rights reserved.
doi:10.1016/j.polymer.2005.05.006

structure is shown in Fig. 1, are imperfect dendritic polymers that may be characterized in terms of a degree of branching (DB), such that DB = 0 for the corresponding linear polymer and DB = 1 for the corresponding perfect dendrimer [19]. Significant exfoliation for MMT contents up to about 20 wt% has been demonstrated in nanocomposites obtained by drying aqueous HBP/MMT suspensions, and this is substantially maintained on subsequent mixing with other components [6,18]. High degrees of exfoliation obtained in this way have been shown to lead to significant improvements in stiffness when the HBP/MMT is introduced into cast PUR thermosets based on polyethylene glycol (PEG) and a commercial diisocyanate hardener [18,20]. On the other hand, they are also associated with large increases in the low strain rate viscosity in the PEG/HBP/MMT precursors [21]. The aim of the present work is to establish a direct link between the precursor characteristics and the low strain response of the final PUR nanocomposites, based on simple geometrical models in which the key parameter is the aspect ratio of the MMT particles.

2. Experimental

The structural parameters of the HBPs, which were provided by Perstorp and will henceforth be referred to by their pseudo-generation number [6], are summarized in Table 1. Given that similar results were generally obtained for the 2 and 4 pseudo-generation HBPs, the focus will be on 2 pseudo-generation HBP in what follows. Unless mentioned otherwise, the required amount of MMT (Na^+MMT from Southern Clay Products, density 2.86 g/cm^3) was first dispersed in the HBP and distilled water. The mixture was stirred in air at about 100 °C until the viscosity had increased to the point, where stirring was no longer possible, and then dried for 3 days at 80 °C under vacuum. The resulting HBP/MMT nanocomposite was either mixed directly at 100 °C for 3 h with PEG of weight average molar mass, M_w = 300 g/mol (Fluka), and stored at 60 °C under vacuum for at least 48 h prior to use, or combined with the PEG in the presence of water, in which case the product was once more carefully dried under vacuum. The PEG/HBP/MMT nanocomposite and a stoichiometric amount of modified diphenylmethane diisocyanate hardener (MDI, M_w = 286 g/mol, average functionality 2.2, from Dow Chemicals) were degassed separately under vacuum at room temperature for 1 h, hand-mixed, poured into a metallic mould and left to react for 5 h in an autoclave at 140 °C and 12 bar.

Glass transition temperatures, T_g, were obtained from differential scanning calorimetry (DSC) heating scans (Perkin–Elmer DSC7) at 10 K/min on 10 mg specimens. Wide angle X-ray scattering (WAXS) measurements on the solid materials were made in reflexion mode using a Siemens Kristalloflex 805 diffractometer. A limited number of measurements were also carried out on liquid PEG/HBP/MMT nanocomposites using a Philips X'Pert diffractometer to avoid tilting the specimens. In each case, the WAXS spectra were recorded at room temperature in the range $2\theta = 1$–$10°$ (Cu K_α, $\lambda = 1.54$ Å). Transmission electron microscopy (TEM) observations were made using a Philips EM430 TEM operated at 300 kV under low dose conditions. Rheological properties were investigated with a Rheometrics ARES (Advanced Rheometric Expansion System) rheometer in oscillating shear with 25 mm diameter parallel plates and a 0.3–0.6 mm gap. All the dynamic rheological measurements were performed at room temperature in the linear viscoelastic regime, whose extent was determined from constant frequency sweeps. Dynamic mechanical analysis (DMA) measurements were made on $50 \times 12 \times 2$ mm^3 bars in three-point bending between −40 and 160 °C at a heating rate of 10 K/min (Rheometrics RSA). Tensile tests were carried out on 2 mm thick dog-bone specimens cut from cast PUR sheets, using a screw

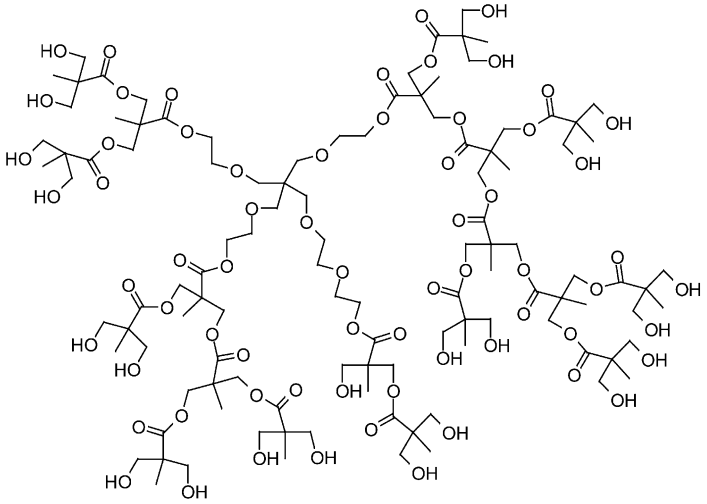

Fig. 1. Representative chemical structure of the HBPs.

Table 1
HBP structural parameters

Designation	M_n (g/mol)[a]	M_n (g/mol)[b]	M_w/M_n[b]	OH-functionality[a]	OH-functionality[c]	DB[d]
2 Pseudo-generation	1747	1130	2.1	16	13	0.30
4 Pseudo-generation	7316	4340	3.2	64	39	0.34

[a] Nominal values based on stoichiometry.
[b] GPC data.
[c] Calculated from NMR.
[d] Degree of branching according to Frey [19].

driven apparatus (UTS Testsysteme GmbH) at 25 and 130 °C, and a crosshead speed of 2 mm/min. The gauge width and length of the tensile test specimens were 5 and 18 mm, respectively, and the nominal strain rate was, therefore, about 1.8×10^{-3} s^{-1}.

3. Results and discussion

The as-received MMT gave a strong WAXS peak at $2\theta = 7.3°$, which corresponds to a platelet spacing, d_{001}, of 1.21 nm. d_{001} increased to 2.52 nm in 2 pseudo-generation HBP/20 wt% MMT, and the WAXS peaks were substantially suppressed at lower MMT contents, which suggested significant exfoliation. Consistent with previous results, d_{001} was slightly higher in 4 pseudo-generation HBP/20 wt% MMT, and exfoliation was again observed at lower MMT contents [6]. For convenience, the effect of PEG on the MMT dispersion was investigated systematically using a relatively high M_w PEG that was solid at room temperature ($M_w = 1500$ g/mol). Fig. 2(a) shows WAXS results for water-processed PEG/2 pseudo-generation HBP blends with 10 wt% MMT. Progressive addition of the HBP led to a gradual decrease in the intensity of the strong WAXS peak at $2\theta \approx 5°$ typical of PEG/MMT nanocomposites obtained by both melt and aqueous processing, and which corresponds to a layer spacing of about 1.76 nm, i.e. intercalation of a monolayer of PEG [22–25]. (For HBP contents greater than 50 wt%, the blends were no longer miscible.) Similar trends were seen in blends containing 5 wt% MMT, as shown in Fig. 2(b). Finally, Fig. 2(c) gives selected WAXS results for the liquid PEG ($M_w = 300$ g/mol)/2 pseudo-generation HBP/MMT nanocomposites, which indicate comparable behavior to that in Fig. 2(a) and (b).

WAXS spectra from PURs obtained by melt mixing the PEG with the HBP/MMT, and then with the MDI, to give an overall matrix HBP content of 10 wt% are shown in Fig. 3(a). These were consistent with the results for the PEG/HBP/MMT precursors in that small WAXS peaks were visible at all compositions at comparable scattering angles to those in Fig. 2. Fig. 3(b) compares the WAXS spectrum from the melt mixed PUR containing 0.6 wt% MMT with that of a PUR for which the PEG and the HBP were mixed in the presence of water and dried prior to mixing with the MDI. This suggests mixing of the PEG/HBP/MMT precursors in the presence of water to increase exfoliation in the PURs. On the other hand, if the HBP was not included in the formulation, the degree of exfoliation was found to be relatively low regardless of the presence of water during mixing. TEM of the PURs confirmed these trends. The PURs prepared from PEG/HBP/MMT mixed in the presence of water showed predominantly exfoliated structures (Fig. 4(a)) with limited platelet stacking (at most one or two layers per stack), and apparent α between about 100 and 200, bearing in mind that the images do not necessarily represent diametrical sections through perfectly circular platelets. In the absence of HBP, on the other hand, MMT particles containing relatively large numbers (50 or more) of coherently stacked individual platelets were visible (Fig. 4(b)) and there was also an apparent increase in the lengths of these particles with respect to those of the exfoliated platelets in Fig. 4(a), possibly owing to shear deformation of the stacks during mixing. α was, therefore, between about 20 and 50, in spite of the extensive stacking. Finally, as shown in Fig. 4(c) and (d) for two different magnifications, PURs prepared by melt mixing the PEG directly with HBP/MMT showed intermediate degrees of exfoliation; relatively large numbers of stacked MMT platelets were again visible locally, but in this case interspersed with isolated platelets.

3.1. Rheological behavior

In constant shear rate experiments on HBP/MMT and PEG/HBP/MMT nanocomposites with relatively high degrees of dispersion, as inferred from the WAXS results, pronounced decreases in viscosity were observed as the shear strain, γ, increased beyond a few percent [20]. Such behavior may be attributed to break-up of a fixed isotropic network of platelets followed by flow induced alignment, consistent with the observation of solid-like behavior in dynamic measurements at low effective shear rates, that is, a finite limiting shear modulus, G_0^*, as the angular frequency $\omega \to 0$ and $\gamma \to 0$. The global dynamic behavior was approximated by

$$\frac{\eta^*}{\eta_\infty^*} \approx 1 + \frac{1}{\sqrt{\omega_r}} + \frac{1}{\omega_r} \quad (1)$$

where the reduced frequency $\omega_r = \eta_\infty^* \omega / G_0^*$ and $\eta_\infty^* \approx \eta_\infty'$ is the limiting shear viscosity as $\omega \to \infty$ and $\gamma \to 0$ [21]. η_∞^* depends strongly on T in these materials through its

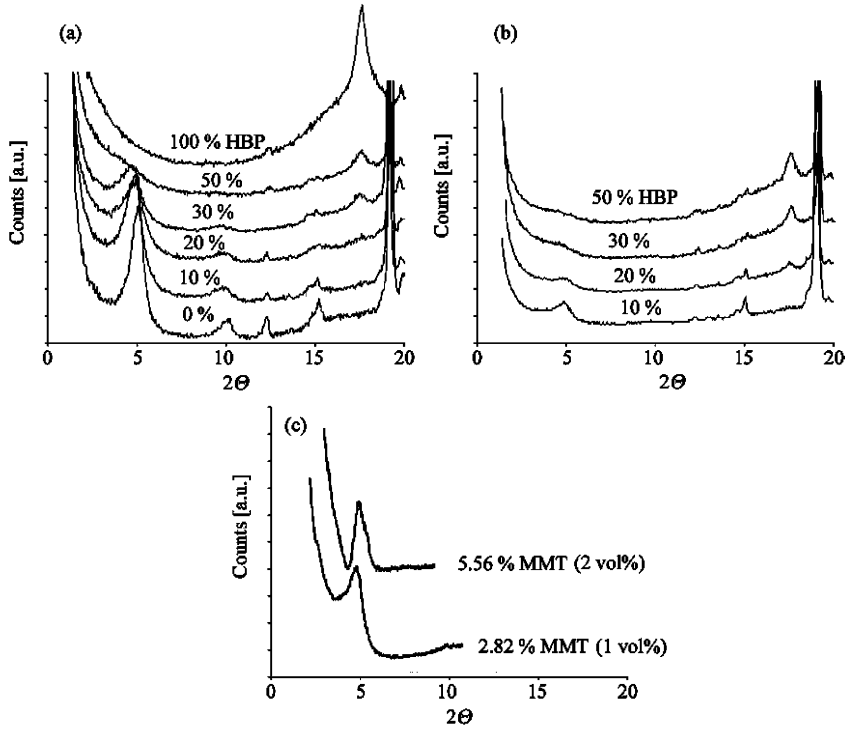

Fig. 2. WAXS results for PEG/2 pseudo-generation HBP/MMT nanocomposites with the matrix HBP weight fractions indicated: (a) PEG (M_w = 1500 g/mol)/HBP/10 wt% MMT; (b) PEG (M_w = 1500 g/mol)/HBP/5 wt% MMT; (c) PEG (M_w = 300 g/mol)/10 wt% HBP with the different MMT contents indicated.

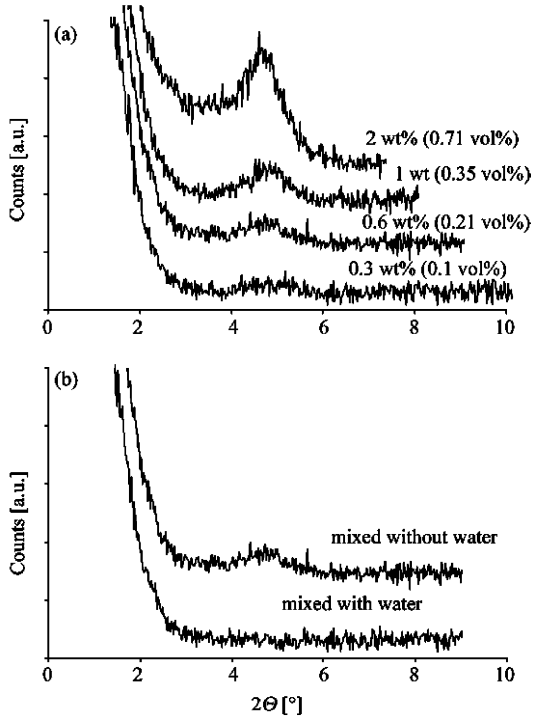

Fig. 3. WAXS results for (a) PURs obtained by using MDI to cure PEG mixed directly with 2 pseudo-generation HBP/MMT with an overall content of 10 wt% HBP, and the MMT contents indicated; (b) PURs containing 0.6 wt% MMT and 10 wt% 2 pseudo-generation HBP in which the PEG and HBP/MMT were (i) mixed in the presence of water and then thoroughly dried prior to cure or (ii) mixed without water.

dependence on the matrix viscosity, η_0, but G_0^* is nearly independent of T. Moreover, G_0^* is a far more rapidly increasing function of the MMT volume fraction, ϕ_1, than η_∞^*, so that it dominates the behavior as ϕ_1 increases, particularly for high degrees of exfoliation. η^* not only increases by orders of magnitude in this regime, but also becomes nearly independent of η_0 and hence of T. This places severe restrictions on the range of ϕ_1 that can be envisaged in practical formulations, because viscosities very much greater than that of the MDI lead to difficulties with mixing.

Data for η^*/η_∞^* for PUR-based nanocomposites with different degrees of exfoliation have been shown to superpose if ϕ_1 is scaled by some constant characteristic of each type of matrix formulation and/or processing route [21]. This may partly be rationalized in terms of classical models for dilute suspensions; simple effective medium arguments for hard particles in a Newtonian fluid lead to

$$\eta = \eta_0 \exp([\eta]\phi_1) \tag{2}$$

for the steady state viscosity in the Brownian limit [26], where η_0 is the matrix viscosity and $[\eta]$ is an intrinsic viscosity, given by

$$[\eta] = \lim_{\phi_1 \to 0} \frac{\eta - \eta_m}{\phi_1 \eta_m} \tag{3}$$

ϕ_1 may be determined from the corresponding weight fraction, w, using

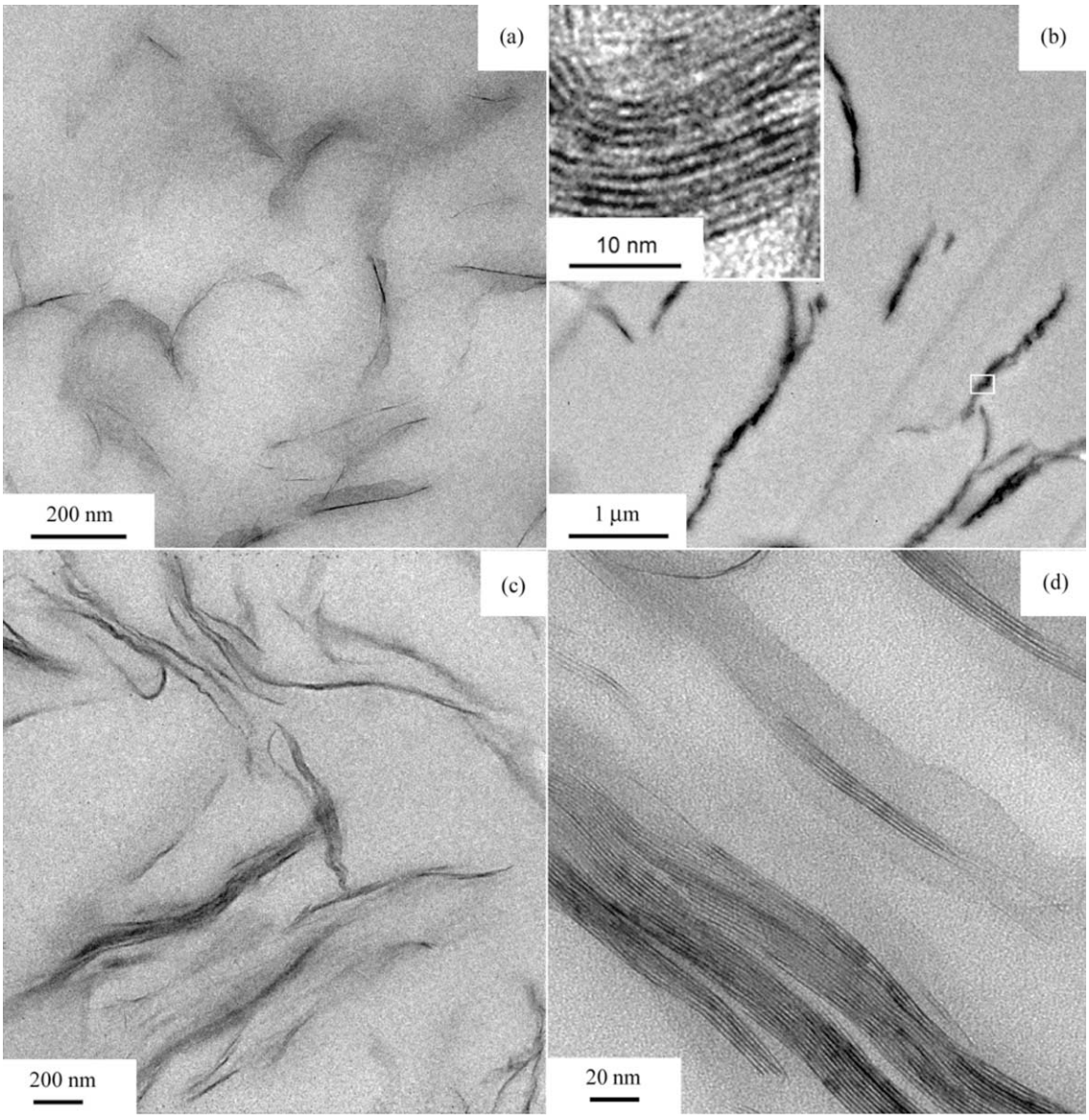

Fig. 4. TEM micrographs of PURs obtained by using MDI to cure (a) PEG/10 wt% 2 pseudo-generation HBP/MMT mixed in the presence of water and dried, overall MMT content of 1.2 wt%; (b) PEG/MMT, overall MMT content of 1.2 wt%; (c) and (d) PEG/10 wt% 2 pseudo-generation HBP/MMT mixed directly, overall MMT content of 2 wt%, at two different magnifications.

$$\phi_1 = \frac{w\rho_{pol}}{w\rho_{pol} + (1-w)\rho_{MMT}}$$

where ρ_{pol} and ρ_{MMT} are the densities of the polymer matrix and the MMT, respectively (ρ_{pol} was approximately 1 g/cm^3 for the precursors in the range of measurement temperatures of interest and approximately 1.1 g/cm^3 for the PUR matrices at room temperature).

In the present case, given that the isotropic distribution of particle orientation is maintained at small deformations, Eq. (2) is assumed to describe the dynamic viscosity in the high strain rate limit, where the platelets behave as non-interacting particles. Models that relate $[\eta]$ and α for isotropic suspensions of spheroidal particles, which approximate to platelets at high α, have been introduced by a number of authors [27–30], and the following representative expression

$$[\eta] = \frac{5}{2} + \frac{32(\alpha-1)}{15\pi} - 0.628\frac{1-\alpha^{-1}}{1-0.075\alpha^{-1}} \quad (4)$$

which simplifies to $[\eta] \approx 0.68\alpha$ for $\alpha \gg 1$, has been verified experimentally for rigid inclusions [31].

Dynamic rheological data are given in Fig. 5(a) for PEG/20 wt% 2 pseudo-generation HBP mixed with different amounts of MMT in the presence of water, showing a strong increase in G^* and η^* with increasing ϕ_1, and the suggestion of a limiting value for η^* at high ω. Where η^* did not reach a plateau, η^*_∞ was estimated by superposing the data in a reduced plot, as described in detail elsewhere [21]. The resulting superposition for the data in Fig. 5(a) is shown in

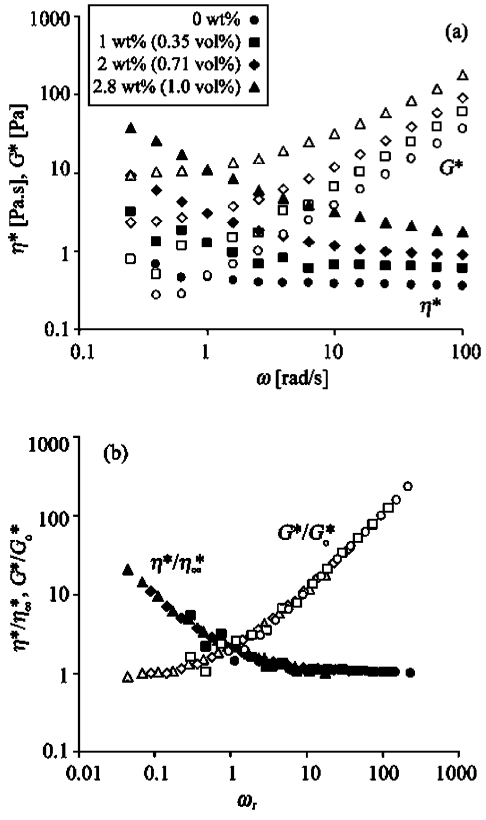

Fig. 5. (a) Complex viscosity η^* and complex modulus G^* versus frequency ω from dynamic shear measurements on 2 pseudo-generation HBP/PEG/MMT nanocomposites mixed in the presence of water and dried with 20 wt% HBP and MMT contents indicted (20 wt% with respect to the PEG gives about 10 wt% HBP in a stoichiometric mixture with the MDI); (b) superposition of reduced rheological data G^*/G_0^* and η^*/η_∞^* versus $\omega\eta_\infty^*/G_0^*$.

Fig. 5(b). [η] was then obtained by substituting η_∞^* for η in Eq. (3) and extrapolating to $\phi_1 = 0$. For the nanocomposites in Fig. 5, [η] was about 128, so that from Eq. (4), $\alpha \approx 188$. Values determined in this way for all the precursors investigated are given in Table 2, from which it may be inferred that α increased significantly in the presence of HBP and by mixing in the presence of water, consistent with the WAXS results.

Eq. (2) not only accounted for the data at low ϕ_1, but also provided a reasonable description of the behavior up to relatively large ϕ_1, whereas the viscosity of a classical suspension might be expected to diverge as ϕ_1 approaches some maximum volume packing fraction, owing to crowding effects. Although the value of the maximum packing volume fraction (the volume fraction beyond which the platelets are no longer able to flow) is not well known even for rigid platelets, the absence of any such threshold would be a natural consequence of the MMT platelets' tendency to align or bend at large ϕ_1. The onset of this behavior may be associated with either a percolation threshold or an overlap concentration. If the silicate layers are taken to act as platelets with an effective aspect ratio α, the percolation threshold ϕ_{per} is given by

$$\phi_{\mathrm{per}} = \frac{9.875\alpha^{-1} + \alpha^{-2}}{7.742 + 14.61\alpha^{-1} + 12.33\alpha^{-3/2} + 1.763\alpha^{-2} + 1.658\alpha^{-3}} \tag{5}$$

or $\phi_{\mathrm{per}} \approx 1.27\alpha^{-1}$ for $\alpha \gg 1$, which is an empirical fit to the results of numerical simulations on randomly oriented ellipsoids of revolution with different aspect ratios [32,33]. This compares with a critical overlap concentration

$$\phi^* = \frac{\pi}{2\alpha} \approx \frac{1.6}{\alpha} \tag{6}$$

for disc-shaped platelets derived from simple excluded volume considerations [34]. ϕ^*, which defines the semi-dilute regime, provides a conservative measure of the range of compositions over which the assumption of randomly oriented, randomly dispersed platelets is strictly valid. Thus, for α of the order of 189 as estimated from the rheological data in Fig. 5, and ϕ_1 greater than about 1 vol%, it is inferred that either local alignment of the platelets must occur, or the platelets must bend in order to reduce their effective α, as sketched in Fig. 6(b) and (c), respectively. The real configuration obtained by drying a relatively dilute isotropic suspension may combine both alignment and reductions in α, depending strongly on the nature of the specific interactions between the platelets. For example, for rigid neutral platelets at equilibrium in a low molar mass matrix and a negative MMT-matrix interaction parameter, application of the equilibrium thermodynamic model of Onsager to discs suggests that nematic ordering, that is local platelet alignment, should occur at ϕ_1 greater than about 0.05 for $\alpha = 100$, and the isotropic phase to disappear altogether at $\phi_1 \approx 0.08$ [34,35]. However, equilibrium theories are likely at best to provide a qualitative indication of the morphologies resulting from drying a suspension. Moreover, for strong specific interactions between the platelets the phase behavior may change radically. A commonly cited case,

Table 2
Comparison of particle aspect ratios inferred from rheological measurements on the nanocomposite precursors and from the plateau modulus of the corresponding polyurethane nanocomposites (HT = Halpin–Tsai, MT = Mori–Tanaka)

Matrix	α (viscosity)	α (modulus/HT)	α (modulus/MT)
HBP/Na^+MMT	527	–	–
HBP/PEG-Na^+MMT[a]	188	150	352
HBP/PEG-Na^+MMT	49	58	135
PEG-Na^+MMT	27	30	71

[a] PEG or ETMP mixed with 2 pseudo-generation HBP/MMT in the presence of water.

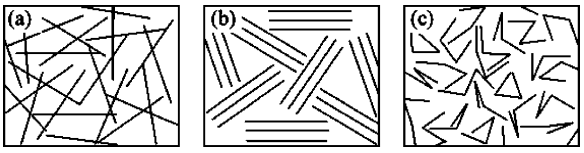

Fig. 6. Two-dimensional representation of the different platelet configurations referred to in the text: (a) random orientation at fixed α; (b) local alignment at fixed α; (c) bending (reduced α).

with direct relevance to MMT, is that of negatively charged platelets with positively charged edges, for which a 'house of cards' arrangement would be favored [1], possibly implying bending rather than alignment to be the dominant mechanism for accommodating high volume fractions of exfoliated MMT, although this is not confirmed unambiguously by TEM micrographs of relatively concentrated HBP/MMT nanocomposites [18].

3.2. Tensile behavior

A number of authors have predicted the elastic constants of MMT reinforced nanocomposites using classical micromechanical models, generally based on a number of simplifying assumptions, with regard to both the morphology (e.g. homogeneously distributed perfectly planar plate-like inclusions) and the properties (e.g. isotropic inclusions with Young's modulus $E_1 = 178$ GPa (by analogy with muscovite mica)) [8,10,36]. In the present case, the cast PUR specimens were assumed to contain randomly oriented and distributed inclusions, although as discussed in the previous section, this may become questionable at large ϕ_1 owing to crowding effects. A first estimate of the stiffness has been obtained from the semi-empirical Halpin–Tsai expressions,

$$E_{11} = E_0 \frac{1 + \zeta\eta\phi_1}{1 - \eta\phi_1} \tag{7}$$

$$\eta = \frac{E_1/E_0 - 1}{E_1/E_0 + \zeta} \tag{8}$$

derived by interpolating numerical solutions for aligned composites [37], where E_0 is the Young's modulus of the matrix and ζ is shape factor that depends on the geometry and orientation of the inclusions. For identical isotropic platelets whose planes are oriented parallel to (x_1, x_2), $\zeta = 2\alpha$. An estimate for the modulus perpendicular to the planes of the platelets, E_{33}, which is insensitive to α, is obtained by setting $\zeta = 2$ in Eqs. (7) and (8). van Es et al. [38] have shown that the reduced Young's modulus of a composite that contains randomly oriented platelets may be approximated to by a linear combination of E_{11} and E_{33} for the corresponding unidirectional composite

$$E = 0.49E_{11} + 0.51E_{33} \tag{9}$$

A more rigorous estimate of the various elastic constants was derived from first principles by applying the Mori–Tanaka average stress theory to a composite that contains ellipsoidal penny-shaped inclusions [39]. This has the advantage of providing explicit expressions for the moduli and may be adapted in a straightforward manner to arbitrary platelet orientation distributions. In the dilute limit (ϕ_1 up to about 5 vol%), the Mori–Tanaka predictions for randomly oriented spheroids are well approximated by the expressions of Norris for the bulk modulus and the effective shear modulus [40],

$$K = K_0 + \frac{4}{9}\phi_1 \left[\frac{\pi}{8\alpha} \frac{3 - 4\nu_0}{\mu_0(1 - \nu_0)} + \frac{1}{\mu_1} \frac{1 - \nu_1}{1 + \nu_1} \right]^{-1} \tag{10}$$

$$\mu = \mu_0 + \frac{1}{15}\phi_1 \left[\frac{\pi}{8\alpha} \frac{3 - 4\nu_0}{\mu_0(1 - \nu_0)} + \frac{1}{\mu_1} \frac{1 - \nu_1}{1 + \nu_1} \right]^{-1} + \frac{2}{5}\phi_1 \left[\frac{\pi}{16\alpha} \frac{7 - 8\nu_0}{\mu_0(1 - \nu_0)} + \frac{1}{\mu_1} \right]^{-1} \tag{11}$$

where ν_0 and ν_1 are the Poisson's ratios of the matrix and MMT, respectively, ($\nu_0 \approx 0.35$ in the glassy state and $\nu_0 \approx 0.5$ in the rubbery state, $\nu_1 \approx 0.2$). For an isotropic material, the elastic constants are related by

$$K = \frac{E}{3(1 - 2\nu)}, \quad \mu = \frac{E}{2(1 + \nu)}, \quad E = \frac{9K\mu}{3K + \mu} \tag{12}$$

The Mori–Tanaka approach has been shown to be consistent with numerical simulations and predicts significantly lower tensile stiffness than the Halpin–Tsai equations at intermediate α [8]. However, these latter will be retained for comparison, because they have been widely employed to model MMT-based nanocomposites in the past. In the present case, as will be seen later, reinforcement in the glassy state was limited over the accessible range of ϕ_1 and discussion will, therefore, focus on the rubbery state, where there was significant reinforcement. In this limit, the above expressions for E may be simplified somewhat. Assuming $E_1 = 178$ GPa and $\phi_1 \ll 1$, and given that E_0 is of the order of MPa, $E_1 \gg \alpha E_0$ for any reasonable choice of α (values up to about 1000). The Halpin–Tsai expression for E_{11} in an oriented composite may then be written

$$E_{11} \approx E_0(1 + \zeta\phi_1) \approx E_0(1 + 2\alpha\phi_1)$$

and from Eq. (9),

$$E \approx 0.49E_0(1 + 2\alpha\phi_1) + 0.51E_0(1 + 2\phi_1) \approx E_0(1 + \alpha\phi_1) \tag{13}$$

for an isotropic composite and $\alpha \gg 1$. In the case of the Mori–Tanaka model, given that $E \approx 3\mu$ in the rubbery state and again assuming $E_1 \gg \alpha E_0$, Eq. (11) implies

$$E \approx E_0 \left(1 + \frac{4\alpha}{3\pi}\phi_1 \right) \tag{14}$$

for small ϕ_1. The modulus is independent of E_1 in Eqs. (13) and (14), because the idealized MMT platelets behave as perfectly rigid reinforcing elements when the matrix is

relatively compliant. It follows that the degree of reinforcement in the rubbery state may be predicted without a precise knowledge of E_1. This is of particular interest in that values as low as 10 GPa have recently been cited for the in-plane modulus of MMT, based on light scattering measurements, which, if verified, would raise questions regarding previous attempts at micromechanical modeling of glassy or semicrystalline nanocomposites [41]. On the other hand, if E_0 and α are taken to be 10 MPa and 500, respectively, say, use of $E_1 = 10$ GPa in Eq. (14) systematically overestimates E by only about 20% with respect to the value given by the full Mori–Tanaka expression.

The evolution of the storage modulus, E', measured by DMA is plotted in Fig. 7(a) for a PUR containing an overall matrix weight fraction of 10 wt% 4 pseudo-generation HBP and different amounts of MMT (similar results were obtained with the 2 pseudo-generation HBP). E' showed little variation with MMT content below T_g, but significant reinforcement was seen at temperatures corresponding to the rubbery plateau. This is shown further in Fig. 7(b), which shows E/E_0 for a series of PURs containing 10 wt% 2 pseudo-generation HBP with different overall MMT contents at temperatures above and below T_g (approximately 35 °C), along with the predictions of the Mori–Tanaka expressions for $\alpha = 135$ and E_1 equal to either 178 or 10 GPa, using the measured E_0 for the matrix indicated in the figure. For comparison, a similar fit of the Halpin–Tsai expression to the data for 130 °C implied α to be about 60.

The experimental scatter in the low temperature data in Fig. 7(b), which may be attributed to variations in matrix properties of different batches, obscured systematic trends in E with ϕ_1. Nevertheless, if E_1 was taken to be 178 GPa and α was adjusted to give a good fit to the data obtained at $T > T_g$, the Mori–Tanaka and the Halpin–Tsai expressions both apparently overestimated the degree of reinforcement at temperatures below T_g. This was not the case if E_1 was taken to be 10 GPa; although the predictions for $T > T_g$ were not significantly affected if the fitted values of α referred to previously were maintained, the predictions for the glassy state, given by the dotted lines in Fig. 7(b), appeared more consistent with the data.

Fig. 8 summarizes further data for E/E_0 obtained at $T > T_g$ in different PUR nanocomposites as a function of ϕ_1, along with fits of Eq. (14) obtained by adjusting α. The α values derived in this way are given in Table 2 along with estimates of α from Eq. (13) (Halpin–Tsai). Both sets of values were clearly correlated with the α values inferred from the rheological measurements. However, the Mori–Tanaka model gave significantly larger absolute values of α than these latter. The assumptions that long range interactions do not contribute to the melt response, and that the high ω plateau in dynamic rheological measurements is equivalent to the low strain rate plateau in steady state data are clearly questionable. However, the implied α of about 200 at high degrees of exfoliation and low ϕ_1, say, appeared more consistent with direct observation by TEM

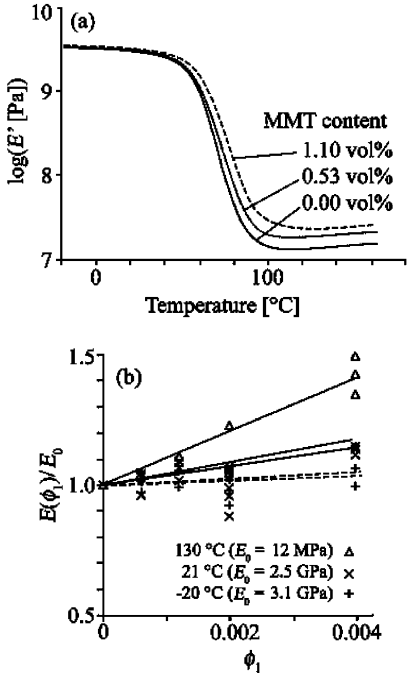

Fig. 7. (a) DMA data for E' as a function of temperature for a PUR containing 15 wt% 4 pseudo-generation HBP and 0, 0.53 and 1.1 vol% MMT; (b) E/E_0 measured at different temperatures in PURs containing PEG/10 wt% 2 pseudo-generation HBP as a function of MMT content; the solid curves are the predictions of the Mori–Tanaka model for $E_1 = 178$ GPa and $\alpha = 135$. The dotted curves were obtained taking $E_1 = 10$ GPa.

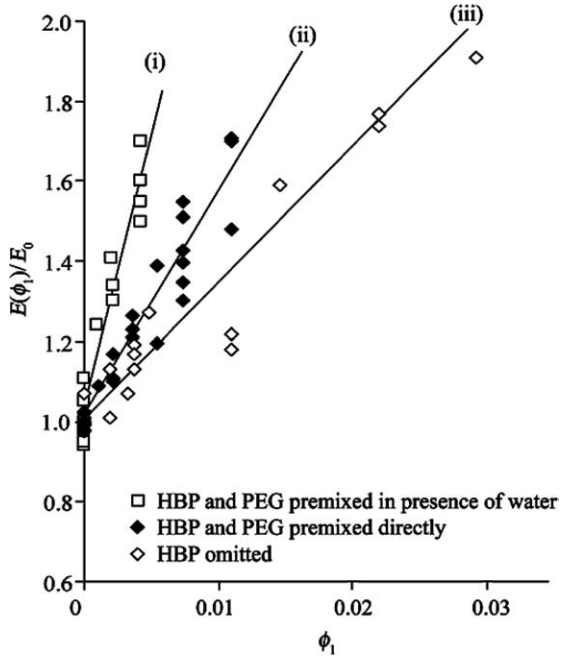

Fig. 8. E/E_0 measured for various polyurethane matrices as a function of MMT content at $T > T_g$, that is, 130 °C (10 wt% 2 pseudo-generation HBP/PEG/MDI, $E_0 = 17$ MPa) and 100 °C (PEG/MDI, $E_0 = 15$ MPa); the solid curves are Mori–Tanaka predictions for (i) $\alpha = 150$, (ii) $\alpha = 70$ and (iii) $\alpha = 30$, E_0 appropriate to the corresponding matrices as indicated in the figure.

(Fig. 4(a)) than the value of 352 inferred from the Mori–Tanaka model. Indeed, given that the real MMT platelets are not perfectly rigid, one might expect the values derived from micromechanical models for the composite the stiffness to be underestimates (platelet buckling will tend to favor lateral contraction, for example).

Another possible explanation for these apparent inconsistencies is that the rubber network is altered by the presence of the filler in the rubbery state (in the glassy state the stiffness is dominated by relatively short range interactions [42]). By analogy with the effect of carbon black, say, on rubber networks, it would be reasonable to expect the effective cross-link density to increase with the surface to volume ratio of the MMT, that is, to be proportional to α, at least in the dilute limit. In the absence of direct mechanical reinforcement this would lead to

$$E \approx E_0(1 + \rho\alpha\phi_1) \tag{15}$$

where ρ is a constant related to the effective increase in cross-link density due to the MMT. Hence, if one takes into account the reinforcing effect of the MMT (and the micromechanical models suggest this to be necessary even for relatively modest α) one obtains

$$E \approx E_0(1 + \xi\alpha\phi_1)(1 + \rho\alpha\phi_1)$$

$$\approx E_0\left(1 + \alpha(\xi + \rho)\phi_1 + \rho\xi\alpha^2\phi_1^2\right) \tag{16}$$

where ξ is of the order of unity, depending on the choice of micromechanical model (cf. Eqs. (13) and (14)). However, although a non-linear dependence of the stiffness on ϕ_1 might in principle be tested for, in the present case, a close to linear dependence on ϕ_1 is predicted for the accessible range of data, making it difficult to discriminate between effects relating to network modification and inaccurate estimates of parameters such as E_1.

The high strain behavior of the PURs was also strongly dependent on T. In PURs containing an overall weight fraction of 10 wt% HBP melt mixed with the PEG and tested at room temperature (below T_g), where E showed little dependence on MMT content, the stress reached a local maximum at a few % strain, defined conventionally as the yield stress, σ_y. Higher HBP contents led to brittle failure in the elastic domain before yielding could occur. σ_y increased by about 10% on addition of 1 wt% MMT, as shown in Figs. 9(a) and 10. Again, similar results were obtained for 2 pseudo-generation HBP as also shown in Fig. 10. Beyond the yield point, pronounced strain softening occurred, followed by necking over the whole gauge length at roughly constant force and finally strain hardening for $\varepsilon \gg 0.2$. The necking was accompanied by stress whitening, believed to be due to cavitation associated with unexfoliated MMT particles oriented at high angles to the tensile axis. Although the elongation at break, ε_r, increased somewhat at 1 wt% MMT, as the amount of MMT was increased further, the specimens became more brittle, as observed previously by Tortora et al. [43] and Plummer et al. [6] on MMT/PUR

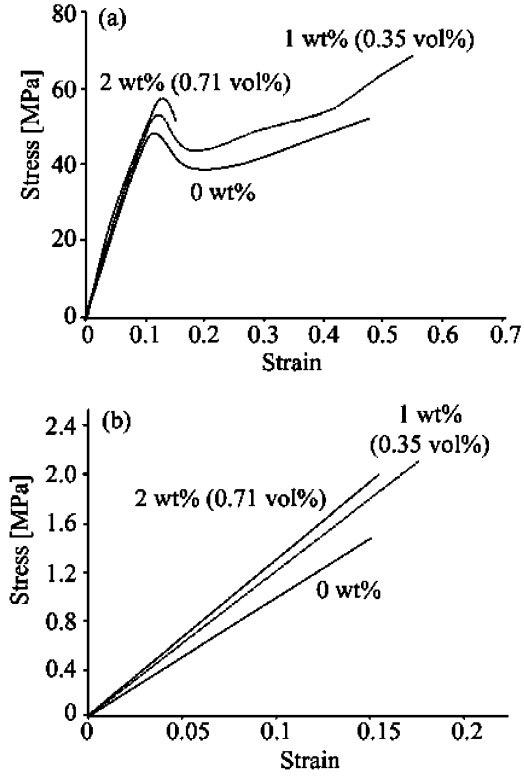

Fig. 9. Nominal stress–strain curve of PUR containing 10 wt% of 4 pseudo-generation HBP at 0, 1 and 2 wt% of MMT (a) at $T = 25$ °C and (b) at $T = 130$ °C.

nanocomposites. At 130 °C (well above T_g), the PURs containing 10 wt% HBP showed an elastomeric response, as shown in Fig. 9(b). As in the glassy state, there was some improvement in ε_r at MMT contents of the order of 1 wt%, but it began to fall off at higher MMT contents.

As well as the apparent limitations on ultimate properties above a certain threshold MMT content, it may be inferred from the discussion in connection with Eq. (6) that the elastic properties can no longer be described in terms of a simple isotropic model composite for $\phi_1 > \phi^*$. This is difficult to test experimentally, because, as pointed out earlier, processing is no longer straightforward in this regime. However, it is useful to estimate the consequences of packing constraints in order to assess the extent to which

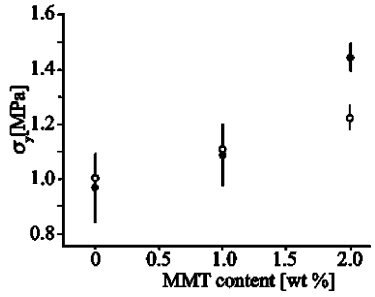

Fig. 10. Influence of the MMT content on the reduced yield stress at $T = 25$ °C in specimens whose matrix contained 10 wt% HBP (open symbols, 2 pseudo-generation HBP; filled symbols, 4 pseudo-generation HBP).

it is worth attempting to overcome these processing difficulties. This has been done very approximately by assuming a uniform reduction in α (by bending of the platelets) throughout the composite for $\phi_1 > \phi^* \approx 1.6/\alpha$ so that the effective aspect ratio for $\phi_1 > \phi^*$ is equal to $1.6/\phi_1$. Alternatively, α may be assumed to remain constant (rigid platelets), and the platelets to align locally to give stacks containing an average number

$$\bar{N} = 1, \quad \phi_1 \leq \phi^* \tag{17}$$

$$\bar{N} = \alpha\phi_1, \quad \phi_1 > \phi^*$$

of platelets. Either approach leads to very similar results for any reasonable choice of layer spacing [32], although the interpretation of non-integral $\bar{N}$ in a model based on identical inclusions is open to question. In the limit $E_1 \gg \alpha E_0$ and $\phi_1 > 1.6/\alpha$, Eq. (14) implies $E \approx 1.68E_0$, regardless of ϕ_1. The implication is, therefore, that there is relatively little to be gained from adding volume fractions of unoriented platelets greater than ϕ^*, if the object of MMT addition is stiffness reinforcement. Another issue of particular relevance to thermosets, particularly in view of the effect of the MMT on rheological properties, is the extent to which the MMT is homogeneously dispersed after mixing with the diisocyanate hardener. Domains rich in high α platelets, but for which the local value of $\phi_1 \gg \phi^*$, are likely to be particularly inefficient at reinforcing the composite for the reasons discussed above. This effect may be estimated by assuming the MMT to be restricted to a volume fraction ϕ' of equiaxed domains. This latter is a reasonable assumption given that the component containing the MMT is expected to be more viscous than the hardener. In the absence of any restrictions on orientation at high α, small amounts of inhomogeneity, that is, relatively large ϕ', lead to relatively small decreases in E. However, if α is taken to be $1.6/\phi_1$ for $\phi_1 \gg \phi^*$, E becomes more sensitive to the state of dispersion, decreasing approximately linearly with decreasing ϕ'. Moreover, inhomogeneous platelet distributions would also imply poor mixing of the hardener with the polyol, so that deviations from stoichiometry may also result in relatively low E_0.

4. Conclusions

It has been shown that the particle aspect ratios inferred from classical models for the viscosity of PEG/HBP/MMT precursors are correlated with those derived from micromechanical models for the low strain response of the corresponding cast PUR thermosets. The implication is that the MMT dispersions in the PURs reflect those of the precursors, so that improvements in the low strain stiffness can only be obtained at the cost of an increase in viscosity and hence reduced processability. On the other hand, it is argued that the assumption of isotropic MMT particle orientation implies a progressive reduction in the effective particle aspect ratio, and hence only minor additional increases in stiffness with MMT content beyond a threshold that decreases with the observed MMT particle aspect ratio in the limit of low concentration, and corresponds roughly to the limit of processability. Optimum specific stiffness in isotropic nanocomposites in terms is, therefore, inferred to be restricted to very low MMT contents, depending on the degree of exfoliation or the extent to which the aspect ratios of unexfoliated MMT particles increase as a result of shear deformation during mixing, for example. This clearly has important practical consequences. However, quite apart from the issue of particle orientation during processing, which is not addressed here, the models on which these ideas are based involve substantial simplifications and, although correlations are observed between the particle aspect ratios derived in different ways, there are significant differences in their absolute values. More systematic morphological characterization is, therefore, required in order to determine, for example, whether (i) the assumption of constant MMT particle aspect ratios at low concentrations is justified; (ii) the MMT dispersion is maintained during processing; (iii) the observed phenomena are scale independent, and hence consistent with a simple classical approaches adopted here.

Acknowledgements

Thanks are due to the Swiss Technically Oriented Program (TOP) ‘Nano 21’ and Dow Europe for their financial support, the members of the Centre Interdisciplinaire de Microscopie Electronique (CIME) of the EPFL for their technical assistance, Dr Kurt Schenk of the Laboratoire de Cristallographie of the EPFL for his help with the WAXS measurements, Prof P. Gudmundson for valuable discussions and Thomas Studer for his contributions to the tensile and rheological measurements.

References

[1] Alexandre M, Dubois P. Mater Sci Eng R-Rep 2000;28(1/2):1–63.
[2] Kojima Y, Usuki A, Kawasumi M, Okada A, Fukushima Y, Kurauchi T, et al. J Mater Res 1993;8(5):1185–9.
[3] Kim YK, Choi YS, Wang MH, Chung IJ. Chem Mater 2002;14(12):4990–5.
[4] Hasegawa N, Kawasumi M, Kato M, Usuki A, Okada A. J Appl Polym Sci 1998;67:87–92.
[5] Chen TK, Tien YI, Wei KH. Polymer 2000;41(4):1345–53.
[6] Plummer CJG, Garamszegi L, Leterrier Y, Rodlert M, Månson J-AE. Chem Mater 2002;14(2):486–8.
[7] Okada A, Usuki A. Mater Sci Eng C—Biomimetic Mater Sens Syst 1995;3(2):109–15.
[8] Sheng N, Boyce MC, Parks DM, Rutledge GC, Abes JI, Cohen RE. Polymer 2004;45(2):487–506.
[9] Ji XL, Jing JK, Jiang W, Jiang BZ. Polym Eng Sci 2002;42(5):983–93.

[10] Luo JJ, Daniel IM. Compos Sci Technol 2003;63(11):1607–16.
[11] Manias E, Touny A, Wu L, Strawhecker K, Lu B, Chung TC. Chem Mater 2001;13(10):3516–23.
[12] Strawhecker KE, Manias E. Chem Mater 2000;12(10):2943–9.
[13] Vaia RA, Giannelis EP. Macromolecules 1997;30(25):7990–9.
[14] Hu Y, Song L, Xu J, Yang L, Chen Z, Fan W. Colloid Polym Sci 2001; 279(8):819–22.
[15] Wang Z, Pinnavaia TJ. Chem Mater 1998;10(12):3769–71.
[16] Ma J, Zhang S, Qi Z. J Appl Polym Sci 2001;82:1444.
[17] Tien YI, Wei KH. Macromolecules 2001;34(26):9045–52.
[18] Rodlert M, Plummer CJG, Garamszegi L, Leterrier Y, Grünbauer HJM, Månson J-AE. Polymer 2004;45(3):949–60.
[19] Holter D, Burgath A, Frey H. Acta Polym 1997;48(1/2):30–5.
[20] Rodlert M, Plummer CJG, Grünbauer HJM, Månson J-AE. Adv Eng Mater 2004;6(9):715–9.
[21] Rodlert M, Plummer CJG, Leterrier Y, Grünbauer HJM, Månson J-AE. J Rheol 2004;48(5):1049–66.
[22] Shen ZQ, Simon GP, Cheng YB. Polym Eng Sci 2002;42(12):2369–82.
[23] Vaia RA, Sauer BB, Tse OK, Giannelis EP. J Polym Sci Part B: Polym Phys 1997;35(1):59–67.
[24] Ogata N, Kawakage S, Ogihara T. J Appl Polym Sci 1997;66(3): 573–81.
[25] Wu JH, Lerner MM. Chem Mater 1993;5(6):835–8.
[26] Larson RG. The structure and rheology of complex fluids. New York: Oxford University Press; 1999.
[27] Barnes HA, Hutton JF, Walters K. An introduction to rheology. Amsterdam: Elsevier; 1989.
[28] Brenner H. Int J Multiphase Flow 1974;1:195–341.
[29] Guven N. Clay–water interface and its rheological properties. Boulder, CO: The Clay Minerals Society; 1992.
[30] Kuhn W, Kuhn H. Helvetica Chim Acta 1945;28(1):97–127.
[31] van der Kooij FM, Boek ES, Philipse AP. J Colloid Interf Sci 2001; 235:344–9.
[32] Bicerano J, Douglas JF, Brune DA. J Macromol Sci-Rev Macromol Chem Phys 1999;C39(4):561–642.
[33] Garboczi EJ, Snyder KA, Douglas JF, Thorpe MF. Phys Rev E 1995; 52(1):819–28.
[34] Lyatskaya Y, Balazs AC. Macromolecules 1998;31(19):6676–80.
[35] Onsager L. Ann NY Acad Sci 1949;51(4):627–59.
[36] Fornes TD, Paul DR. Polymer 2003;44(17):4993–5013.
[37] Halpin JC, Kardos JL. Polym Eng Sci 1976;16(5):344–52.
[38] van Es M, Xiqiao F, van Turnhout J, van der Giessen E. Comparing polymer–clay nanocomposites with conventional composites using composites modeling. In: Al-Malaika S, Golovoy AW, editors. Specialty polymer additives: principles and applications. Oxford: Blackwell Science; 2001 [Chapter 21].
[39] Tandon GP, Weng GJ. Polym Compos 1984;5(4):327–33.
[40] Norris AN. Int J Solids Struct 1990;26(5/6):663–74.
[41] Giannelis E. Presented at the ECCM 11, Rhodes; 2004.
[42] Brechet Y, Cavaille JYY, Chabert E, Chazeau L, Dendievel R, Flandin L, et al. Adv Eng Mater 2001;3(8):571–7.
[43] Tortora M, Gorrasi G, Vittoria V, Galli G, Ritrovati S, Chiellini E. Polymer 2002;43(23):6147–57.